ChemComm

Single-molecule determination of chemical equilibrium of DNA intercalation by electrical conductance

Journal:	*ChemComm*
Manuscript ID	CC-COM-12-2020-008348.R1
Article Type:	Communication

COMMUNICATION

Single-molecule determination of chemical equilibrium of DNA intercalation by electrical conductance

Received 00th January 20xx,
Accepted 00th January 20xx

DOI: 10.1039/x0xx00000x

Lu Zhang, Satoshi Kaneko, Shintaro Fujii, Manabu Kiguchi, and Tomoaki Nishino*

We investigated a single-molecule reaction of DNA intercalation as an example of a bimolecular association reaction. Single-molecule conductance values of the product and reactant molecules adsorbed on an Au surface were measured to identify and quantify these molecules. The binding isotherm was constructed, and the association constant of the reaction was determined on a single-molecule basis.

In the past decades, considerable advances have been made to analyze a single molecule and to explore the single-molecule phenomenon.[1-3] A representative example of such an investigation is molecular electronics,[4,5] wherein a single molecule is utilized as an electronic component, e.g., single-molecule switches,[6] diodes,[7] and transistors.[8] Furthermore, the development of single-molecule science has spurred the investigation of a chemical reaction at the single-molecule level.[9-11] Tracing reactions occurring in a single molecule or between single molecules can offer insights into mechanistic knowledge overlooked in conventional ensemble measurements. For example, single-molecule studies can reveal stochastic fluctuations of a reaction at its equilibrium and can help to directly map the reaction potential surface. These insights, offered by the observation of the single-molecule reaction, lead to an exploration of novel chemical transformations.

Single-molecule junctions have been widely utilized in the investigation of the electronic properties of a single molecule. A molecular junction is prepared by embedding the target molecule into a nanogap between electrodes based on the break-junction technique using scanning tunneling microscopy (STM-BJ)[12,13] or on the mechanically-controllable break junction[14-16] technique. The electrical conductance of a single molecule has been extensively studied using a molecular junction to develop single-molecule devices.[17] Moreover, the electron-transport properties of a molecular junction are largely affected by the chemical identity of the molecule in the junction.[5] This effect opens a way for the sensing application of single-molecule junctions, which achieves a single-molecule sensitivity, together with a label-free electrical detection like field-effect transistor sensors.[18,19]

Besides the sensing applications, it is anticipated that single-molecule junctions offer an opportunity to investigate single-molecule reactions by detecting the molecular transformations concomitant to the chemical reaction of embedded molecule. Guo and co-workers successfully studied the kinetics of a nucleophilic addition reaction of a single molecule by using a stable molecular junction based on graphene electrodes.[20] We recently studied a DNA hybridization reaction using molecular tips of nucleic acids to reveal the reaction kinetics at the single-molecule level.[21] From a kinetic perspective, significant advances have been made in single-molecule reactions, as exemplified above. However, the thermodynamic description of a single-molecule reaction still remains elusive.[22,23]

In the present study, we developed a methodology to argue the thermodynamics of single-molecule reactions based on the quantification of single molecules. Single-molecule detection by electrical measurements using STM-BJ was applied to the reaction of the intercalation of a dye molecule, ethidium bromide (EB), to double-stranded DNA as an example of a bimolecular association reaction. The intercalation reactions of this kind have been utilized in a wide range of applications, including bioassays, therapeutic treatments, and creation of functional nanostructures.[24,25] Distinct differences were found in the single-molecule conductance values of the product (EB–DNA complex) and reactants (EB and DNA). Consequently, the present electrical measurements enabled the discrimination and quantification of each chemical species for the thermodynamic analysis. The present research offers a novel way for the thermodynamic description of a single-molecule reaction, which would provide the energetic perspectives of such reactions. It has been demonstrated that the electronic

Department of Chemistry, School of Science, Tokyo Institute of Technology Ookayama, Meguro-ku, Tokyo 152-8551, Japan. E-mail: tnishino@chem.titech.ac.jp

†Electronic Supplementary Information (ESI) available. See DOI: 10.1039/x0xx00000x

structure of a molecule, which plays a decisive role in chemical reactions, is significantly altered when the molecule is embedded in the junction.[26] We, therefore, expect that the present method leads to exploration of novel reactivities of molecules in the nanogap between metal electrodes.

We addressed the equilibrium of a complexation reaction between DNA and EB on a single-molecule basis (Fig. 1a). Double-stranded DNA (5'-GCTTGTTG-3' and its complementary strand) served as the sample, and the thermal stability of the DNA was confirmed by measuring the melting temperature (Fig. S1, ESI†). A thiol-containing linker group, i.e., -$(CH_2)_3$SH, was introduced at the 3' terminal of each strand for the chemisorption of the duplex on the substrate and the STM tip via S–Au bonding. First, the single-molecule conductance values of each reactant and product, i.e., DNA, EB, and EB–DNA complex, was determined using the STM-BJ technique in air at room temperature. The Au STM tip was first driven to approach the Au(111) substrate modified with the target molecule under ambient conditions. When the tip was pulled away from the substrate, the conductance, calculated from the tunneling current, was recorded as a function of tip displacement (see ESI† for the experimental procedures). The resulting conductance traces obtained using an Au substrate modified by immersion in a 0.1 M PBS solution containing 1.0 μM DNA exhibited characteristic plateaus (Fig. 1b, inset). The plateaus indicate the formation of single-molecule junctions.[12] For statistical analysis, thousands of traces were integrated to construct the conductance histogram (Fig. 1b). An obvious peak characterizes the histogram, which corresponds to the most probable conductance of the junction. The conductance of the present single-molecule junction of DNA was determined to be 2.5×10^{-4} G_0, where G_0 stands for the conductance quantum and equals to $2e^2/h$ (*e* and *h* are elementary charge and the Planck constant, respectively).

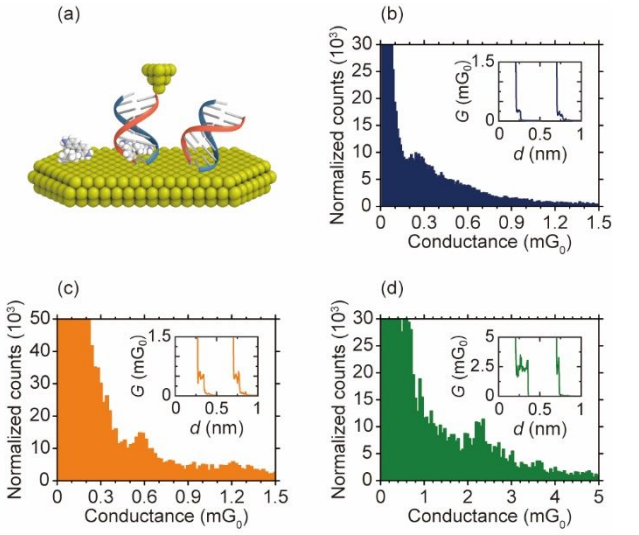

Fig. 1 (a) Schematic of measurements of single-molecule conductance. Au substrates modified with DNA, EB, or mixture of DNA, EB, and EB–DNA complex served as sample surfaces. Conductance histogram for the single-molecule junctions of (b) free DNA, (c) EB, and (d) EB–DNA from STM-BJ measurement under a bias voltage of −50 mV. Insets show respective representative conductance traces. The histograms of b, c, and d were created from 1385, 1684, and 1253 traces, respectively.

Similar STM-BJ studies were performed with the substrate immersed in a PBS solution containing 1.0 μg/ml EB and in a PBS solution containing both 1.0 μM DNA and 1.0 μg/ml EB (Fig. 1c and 1d, respectively). Consequently, the single-molecule conductance of EB and DNA–EB complex was consequently determined to be 6.1×10^{-4} G_0 and 2.2×10^{-3} G_0, respectively (see ESI† for detailed discussions), both of which is in accordance with our earlier report.[27]

The single-molecule conductance values of the chemical species relevant to the complexation reaction were successfully determined using the STM-BJ technique, and the distinct differences among them help identify a single molecule based on the electrical measurements. Thus, the single-molecule conductance was utilized to determine the equilibrium constant of the complexation reaction. The substrate immersed in the mixed solution of 1.0 μM DNA and 1.0 μg/ml EB served as the sample substrate. The substrate was immediately blown dry after immersion to preserve the equilibrium state, that is, the ratio of the product to the unreacted reactants, in the solution. To measure the probabilities of finding the reactants and products on the surface, the formation of the single-molecule junction was monitored in the time domain by current–time (*I*–*t*) measurements.[28,29] Unlike the STM-BJ measurement, the STM tip was frozen above the sample surface at a constant distance with the STM feedback disabled, and the current was recorded as a function of time. Data were continuously recorded without involving the tip movements. In this way, large datasets can be obtained easily, leading to statistically robust analyses.

Fig. 2a shows the representative *I*–*t* traces obtained using the Au(111) substrate modified with a mixed solution containing 1.0 μM DNA and 1.0 μg/ml EB. Sudden increases in the tunneling current over the stable background current were repeatedly observed. These current jumps arise due to the spontaneous formation of single-molecule junctions.[28-30] Thus, single-molecule conductance can be estimated based on the increasing current values relative to the set-point current. The traces exhibited a variety of conductance values, as seen in Fig. 2a, indicating the formation of more than one type of molecular junction. In the short time period as in Fig. 2a, plateaus showing the similar conductance appeared, but those with a variety of conductance were observed for a longer duration. To statistically determine the conductance, 6000 traces were analyzed to extract the current jumps using an automated algorithm, i.e., adaptive threshold analysis,[31] and the conductance histogram was constructed as shown in Fig. 2b. Three distinct conductance groups appeared in the histogram: a low-conductance group at 2.5×10^{-4} G_0; a medium-conductance group at 7.6×10^{-4} G_0; and a high-conductance group at 2.8×10^{-3} G_0. The conductance of each group reasonably agrees with the conductance determined using the STM-BJ technique (Fig. 1), and we ascribe the low-, medium-, and high-conductance groups to the formation of single-molecule junctions accommodating DNA (blue), EB (orange), and EB–DNA complex (green), respectively.

We prepared more samples where the substrates were immersed in solutions with various concentrations of EB. These

samples were then subjected to *I*–*t* measurements. Current traces similar to those in Fig. 2a were obtained, and the three states appeared again in the resulting conductance histograms (see Fig. 2c for the analysis where 10 μg/ml EB was used and see Fig. S2 in ESI† for other examples). The conductance value of each state in reasonable agreement with the one observed in Fig. 2b (Table S1, ESI†). However, the peak intensities were found to be dependent on the EB concentration (Fig. S3, ESI†). A comparison between Fig. 2b, 2c, and Fig. S2 in ESI† shows that the peak intensity of the low-conductance state notably decreased as the EB concentration increased. In contrast, the intensities of both the medium- and high-conductance states decreased with an increase in the EB concentration. The chemical assignment of each conductance state explains the intensity changes. With low EB concentration (e.g., Fig. 2b), the content of unreacted DNA (assigned to the low-conductance state) increases, while the excess amount of EB (e.g., Fig. 2c) results in an increase in the content of EB–DNA complex and unreacted EB (high- and medium-conductance states, respectively). We found in the previous study that the single-molecule conductance of DNA junctions does not depend on the surface coverage of DNA,[32] which assures the results of the present measurements involving the sample surfaces with different DNA coverages.

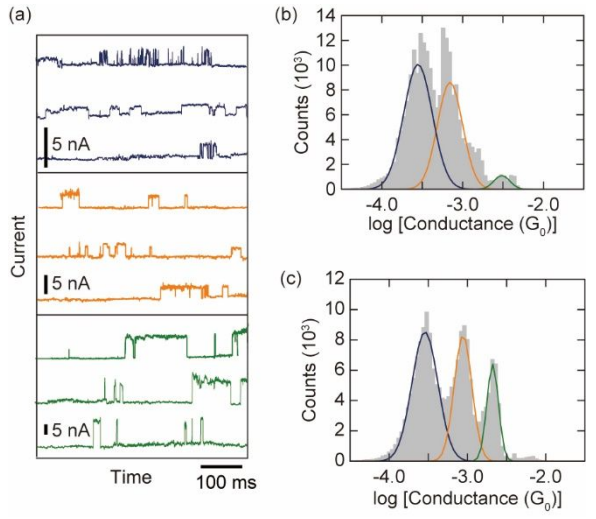

Fig. 2 (a) Current traces and (b) conductance histogram acquired by *I*–*t* measurements using substrate modified in the solution of 1.0 μM DNA and 1.0 μg/ml EB. (c) Conductance histogram obtained by *I*–*t* measurements. The solution of 1.0 μM DNA and 10 μg/ml EB was used for substrate modification. Bias voltage of 50 mV and set-point current of 5 nA were employed for the *I*–*t* measurements. Both the histograms of b and c were compiled from 6000 traces.

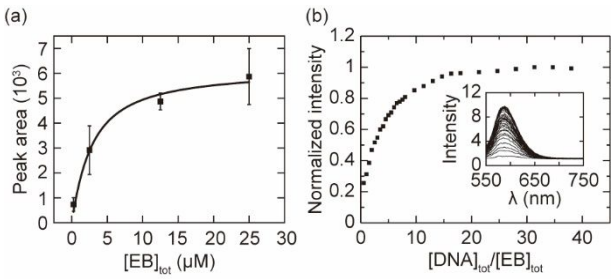

Fig. 3 (a) Plot of peak area for EB–DNA junction of conductance histogram, obtained by *I*–*t* measurements, as a function of total EB concentration. (b) Plot of fluorescence intensity at λ_{max} as a function of total DNA concentration. Fluorescence and DNA concentrations were normalized by maximum fluorescence intensity and total EB concentration, respectively. The inset shows fluorescence spectra.

The conductance histograms shown in Fig. 2b and c and Fig. S2 in ESI† show concentration-dependent behavior, and thus, we anticipate that the observed peaks allow for the quantification of the chemical species. The peak area of the conductance histogram corresponds to the sum of the data points included in the plateaus of the current traces. Each plateau arose from the formation of a molecule junction whose observation probability could reflect the number of molecules adsorbed on the sample surface. Hence, the area of the peak corresponding to the EB–DNA single-molecule junction, $S_{EB–DNA}$, can be calculated using the concentration of EB–DNA in the solution used to modify the substrate:

$$S_{\mathrm{EB-DNA}} = \tau P[\mathrm{EB-DNA}] \quad (1)$$

where τ and *P* are the average lifetime and formation probability of the molecule junction, respectively. Meanwhile, the association constant of the present reaction, K_a, is expressed as:

$$K_a = \frac{[\mathrm{EB-DNA}]}{[\mathrm{EB}][\mathrm{DNA}]} \quad (2)$$

Rearrangement using the total concentrations of EB and DNA, $[EB]_{tot}$ and $[DNA]_{tot}$, respectively, and substitution of equation 1 affords the following expression (see also ESI†):

$$S_{\mathrm{EB-DNA}} = \frac{\tau P}{2}\left\{\frac{1}{K_a^{SM}} + [EB]_{tot} + [DNA]_{tot} - \sqrt{\left(\frac{1}{K_a^{SM}} + [EB]_{tot} + [DNA]_{tot}\right)^2 - 4[EB]_{tot}[DNA]_{tot}}\right\} \quad (3)$$

The superscript SM of K_a in equation (3) denotes the single-molecule measurements. Based on the condition that $[DNA]_{tot}$ was kept constant in the experiments reported in Fig. 2 and Fig. S2 in ESI†, the binding curve was constructed using $S_{EB–DNA}$ as a function of $[EB]_{tot}$ (Fig. 3a). Then, the binding isotherm of equation (3) was fitted to the experimental curve via the Levenberg–Marquardt least-squares routine, and consequently, K_a^{SM} of 4.3 × 10^5 M^{-1} was obtained through single-molecule studies. It should be noted that the 1:1 binding mechanism was assumed for the DNA–EB complex in the discussion above, which was rationalized by fluorescence measurements (see below).

We next validated the association constant K_a^{SM} based on the comparison with the corresponding value of the molecular ensemble. Hence, fluorescence spectroscopic studies were performed to investigate the binding between EB and DNA in the solution for obtaining the association constant determined by the conventional ensemble measurement, K_a^{EN}. Apart from the difference in the number of molecules, the comparison between K_a^{SM} and K_a^{EN} involves difference in the measurements on the surface and those in the solution. However, the method to prepare the sample surface ensured that the equilibrium in

the solution was preserved on the surface (see ESI† for the experimental procedures), which allowed for the direct comparison between K_a^{SM} and K_a^{EN}. The 1.0 μM EB solution was titrated against 500 μM DNA solution, and the binding isotherm was obtained based on the maximum fluorescence intensities (Fig. 3b). The fitting of this isotherm yielded K_a^{EN} of 5.0×10^5 M^{-1}. This value is in reasonable agreement with literature,[27] and importantly, the association constant determined by the statistical analysis of the single-molecule measurements, K_a^{SM}, agrees with that deduced by the ensemble measurements, K_a^{EN}. In addition, the analysis of the fluorometric titration indicated that each EB molecule was bound to 0.7 DNA molecule, which validates the assumption of 1:1 binding considered in deriving equation (3). On the basis of the above result, we conclude that the present approach enables the thermodynamic evaluation of single-molecule reactions.

In summary, the measurements of single-molecule conductance were applied to the analysis of a bimolecular association reaction, i.e., the intercalation of EB to DNA. The product and reactants that equilibrated in the bulk solution were immobilized on Au(111) substrates. Definite differences were found in the conductance values of these molecules, which led to the discrimination and quantification of the chemical species. The association constant of the EB intercalation was successfully estimated based on the binding curve derived from the electrical measurements. These results clearly demonstrate that statistical analyses of single-molecule measurements can describe the thermodynamic equilibrium of single-molecule reactions. The methodology described herein can be utilized to shed light on unique thermodynamic perspectives of single-molecule reactions in nanostructures, such as a metal nanogap, which could be distinctly different from those obtained using the conventional ensemble counterpart.

This work was financially Supported by Grants-in-Aid for Scientific Research (No. JP16K14018 and JP18H02003) and JST CREST (No. JP-MJCR18I4) from the Ministry of Education, Culture, Sports, Science and Technology (MEXT) of Japan.

Conflicts of interest

There are no conflicts to declare.

Notes and references

1 A. B. Zrimsek, N. H. Chiang, M. Mattei, S. Zaleski, M. O. McAnally, C. T. Chapman, A. I. Henry, G. C. Schatz and R. P. Van Duyne, *Chem. Rev.*, 2017, **117**, 7583-7613.
2 S. V. Aradhya and L. Venkataraman, *Nat. Nanotechnol.*, 2013, **8**, 399-410.
3 R. Roy, S. Hohng and T. Ha, *Nat. Methods*, 2008, **5**, 507-516.
4 A. Aviram and M. A. Ratner, *Chem. Phys. Lett.*, 1974, **29**, 277-283.
5 T. A. Su, M. Neupane, M. L. Steigerwald, L. Venkataraman and C. Nuckolls, *Nat. Rev. Mater.*, 2016, **1**, 16002.
6 Z. J. Donhauser, B. A. Mantooth, K. F. Kelly, L. A. Bumm, J. D. Monnell, J. J. Stapleton, D. W. Price, A. M. Rawlett, D. L. Allara, J. M. Tour and P. S. Weiss, *Science*, 2001, **292**, 2303.
7 M. Elbing, R. Ochs, M. Koentopp, M. Fischer, C. von Hänisch, F. Weigend, F. Evers, H. B. Weber and M. Mayor, *Proc. Natl. Acad. Sci. U.S.A.*, 2005, **102**, 8815.
8 D.-H. Chae, J. F. Berry, S. Jung, F. A. Cotton, C. A. Murillo and Z. Yao, *Nano Lett.*, 2006, **6**, 165-168.
9 E. Evans, *Annu. Rev. Biophys. Biomol. Struct.*, 2001, **30**, 105-128.
10 Y. Li, C. Yang and X. Guo, *Acc. Chem. Res.*, 2020, **53**, 159-169.
11 X. Zhuang, L. E. Bartley, H. P. Babcock, R. Russell, T. Ha, D. Herschlag and S. Chu, *Science*, 2000, **288**, 2048.
12 B. Xu and N. J. Tao, *Science*, 2003, **301**, 1221.
13 R. Requist, P. P. Baruselli, A. Smogunov, M. Fabrizio, S. Modesti and E. Tosatti, *Nat. Nanotechnol.*, 2016, **11**, 499-508.
14 J. Moreland and J. W. Ekin, *J. Appl. Phys.*, 1985, **58**, 3888-3895.
15 M. A. Reed, C. Zhou, C. J. Muller, T. P. Burgin and J. M. Tour, *Science*, 1997, **278**, 252.
16 D. Xiang, H. Jeong, T. Lee and D. Mayer, *Adv. Mater.*, 2013, **25**, 4845-4867.
17 D. Xiang, X. L. Wang, C. C. Jia, T. Lee and X. F. Guo, *Chem. Rev.*, 2016, **116**, 4318-4440.
18 P. Lin and F. Yan, *Adv. Mater.*, 2012, **24**, 34-51.
19 M. H. Abouzar, A. Poghossian, A. G. Cherstvy, A. M. Pedraza, S. Ingebrandt and M. J. Schöning, *Phys. Status Solidi A*, 2012, **209**, 925-934.
20 J. Guan, C. Jia, Y. Li, Z. Liu, J. Wang, Z. Yang, C. Gu, D. Su, K. N. Houk, D. Zhang and X. Guo, *Sci. Adv.*, 2018, **4**, eaar2177.
21 T. Harashima, Y. Hasegawa, S. Kaneko, Y. Jono, S. Fujii, M. Kiguchi and T. Nishino, *Chem. Sci.*, DOI: 10.1039/D0SC04449K.
22 C. Huang, M. Jevric, A. Borges, S. T. Olsen, J. M. Hamill, J.-T. Zheng, Y. Yang, A. Rudnev, M. Baghernejad, P. Broekmann, A. U. Petersen, T. Wandlowski, K. V. Mikkelsen, G. C. Solomon, M. Brøndsted Nielsen and W. Hong, *Nat. Commun.*, 2017, **8**, 15436.
23 R. J. Brooke, D. S. Szumski, A. Vezzoli, S. J. Higgins, R. J. Nichols and W. Schwarzacher, *Nano Lett.*, 2018, **18**, 1317-1322.
24 M. J. Hannon, *Chem. Soc. Rev.*, 2007, **36**, 280-295.
25 R. Palchaudhuri and P. J. Hergenrother, *Curr. Opin. Biotechnol.*, 2007, **18**, 497-503.
26 Y. Isshiki, T. Nishino and S. Fujii, *J. Phys. Chem. C*, 2021, **125**, 3472-3479.
27 T. Harashima, C. Kojima, S. Fujii, M. Kiguchi and T. Nishino, *Chem. Commun.*, 2017, **53**, 10378-10381.
28 W. Haiss, H. van Zalinge, S. J. Higgins, D. Bethell, H. Höbenreich, D. J. Schiffrin and R. J. Nichols, *J. Am. Chem. Soc.*, 2003, **125**, 15294-15295.
29 W. Haiss, R. J. Nichols, H. van Zalinge, S. J. Higgins, D. Bethell and D. J. Schiffrin, *Phys. Chem. Chem. Phys.*, 2004, **6**, 4330-4337.
30 Y. Hasegawa, T. Harashima, Y. Jono, T. Seki, M. Kiguchi and T. Nishino, *Chem. Commun.*, 2020, **56**, 309-312.
31 T. Harashima, Y. Hasegawa, S. Kaneko, M. Kiguchi, T. Ono and T. Nishino, *Angew. Chem. Int. Ed.*, 2019, **58**, 9109-9113.
32 T. Harashima, Y. Hasegawa, S. Kaneko, Y. Jono, S. Fujii, M. Kiguchi and T. Nishino, *Chemical Science*, 2021, **12**, 2217-2224.